Technical Report Documentation Page

1. Report No.	2. Government Accession No.	3. Recipient's Catalog No.
FHWA/TX-94+1305-1		

4. Title and Subtitle	5. Report Date
FACTORS AFFECTING THE DESIGN THICKNESS OF BRIDGE SLABS: DESIGN AND PRELIMINARY VERIFICATION OF TEST SETUP	*February 1994*
	6. Performing Organization Code

7. Author(s)	8. Performing Organization Report No.
J. H. Whitt, J. Kim, N. H. Burns, and R. E. Klingner	*Research Report 1305-1*

9. Performing Organization Name and Address	10. Work Unit No. (TRAIS)
Center for Transportation Research *The University of Texas at Austin* *3208 Red River, Suite 200* *Austin, Texas 78705-2650*	11. Contract or Grant No. *Research Study 0-1305*
	13. Type of Report and Period Covered *Interim*
12. Sponsoring Agency Name and Address *Texas Department of Transportation* *Research and Technology Transfer Office* *P. O. Box 5051* *Austin, Texas 78763-5051*	14. Sponsoring Agency Code

15. Supplementary Notes

Study conducted in cooperation with the U.S. Department of Transportation, Federal Highway Administration
Research Study Title: "Factors Affecting Design Thickness of Bridge Slabs"

16. Abstract

The punching shear behavior of concrete bridge decks under static, pulsating fatigue, and rolling fatigue loads was studied using both analytical and experimental models. The study of the analytical models also played a large role in the design of the experimental specimens, test setup, and test procedure.

In this report, the development of the test setup is described, and preliminary test results are reported. Complete study results will be discussed in future project reports.

17. Key Words	18. Distribution Statement
concrete bridge decks, bridge slabs, design thickness, punching shear behavior, static, pulsating fatigue, rolling fatigue, loads, analytical and experimental models, specimens, test setup, test procedure	*No restrictions. This document is available to the public through the National Technical Information Service, Springfield, Virginia 22161.*

19. Security Classif. (of this report)	20. Security Classif. (of this page)	21. No. of Pages	22. Price
Unclassified	*Unclassified*	*44*	

Form DOT F 1700.7 (8-72) Reproduction of completed page authorized

FACTORS AFFECTING THE DESIGN THICKNESS OF BRIDGE SLABS: DESIGN AND PRELIMINARY VERIFICATION OF TEST SETUP

by

J. H. Whitt, J. Kim, N. H. Burns, and R. E. Klingner

Research Report Number 1305-1

Research Project 0-1305

Factors Affecting Design Thickness of Bridge Slabs

conducted for the

TEXAS DEPARTMENT OF TRANSPORTATION

in cooperation with the

U.S. DEPARTMENT OF TRANSPORTATION
FEDERAL HIGHWAY ADMINISTRATION

by the

CENTER FOR TRANSPORTATION RESEARCH
Bureau of Engineering Research
THE UNIVERSITY OF TEXAS AT AUSTIN

February 1994

IMPLEMENTATION

This report concerns the development of a testing program and test setup to evaluate the factors affecting the design thickness of bridge slabs. Results of this report have been incorporated into the testing program. They are not intended for other implementation at this time. Implementation of complete study results will be discussed in future project reports.

Prepared in cooperation with the Texas Department of Transportation and the U.S. Department of Transportation, Federal Highway Administration.

Ned H. Burns, Texas P.E. #20801
Richard E. Klingner, Texas P.E. #42483

Research Supervisors

TABLE OF CONTENTS

LIST OF FIGURES

SUMMARY

The punching shear behavior of concrete bridge decks under static, pulsating fatigue, and rolling fatigue loads was studied using both analytical and experimental models. The study of the analytical models also played a large role in the design of the experimental specimens, test setup, and test procedure.

Two primary models were analyzed using the finite element method. The first model was a finite element mesh representing a full-size, realistic highway bridge. The prototype was a 50-foot-span (15.24 m), three-girder bridge with a 7½-inch (191 mm) concrete deck. Solid elements, or 8-node brick elements, were used to model the concrete deck, while frame elements, or 2-node beam-column elements, were used to model the girders. This full-size bridge model was loaded in a typical AASHTO design truck loading pattern.

The second model represented the actual slab specimen to be tested in the laboratory. The full-scale specimen measured 6 feet (1.83 m) wide, 7 feet (2.13 m) long, and 7½ (191 mm) inches thick, and was modeled using 8-node solid elements. Loading of the specimen model emulated the loading used in the experiment, which, in turn, was representative of an actual truck tire footprint.

When both models -- the full-size bridge model and the experimental specimen model -- were analyzed, it was observed that similar arching action behavior occurred in each, despite different geometries and load configurations. Also, it was possible to find out from the specimen model exactly how far a rolling load would have to move in order to obtain satisfactory fatigue behavior in the slab.

The steel testing frame for this project was designed for three different types of test: static loading, pulsating fatigue, and rolling fatigue. The static tests consisted of monotonically loading a full-scale slab until a punching shear failure occurred. The pulsating tests were very similar, but the load varied in magnitude, cycling until a punching shear failure occurred in the slab. The setup for the rolling tests was slightly different, allowing a constant load to be moved longitudinally across the slab, cycling until failure. Both types of fatigue tests were controlled through closed-loop servo-controllers and hydraulic loading systems.

As this report was being finalized, one complete static test had been completed. More static load tests, as well as several fatigue tests, are scheduled to be performed and will be discussed and analyzed in future reports.

CHAPTER 1
INTRODUCTION

1.1 General

Experimental research represents a vital concept in all engineering disciplines — the concept that theoretical ideas can be explicitly proven to be applicable to the real, physical world. This concept is important to the academic world as well as the practical one. Therefore, a researcher must prove that an experimental model directly relates to the real world situation that it is intended to represent. This is done by conducting thorough analyses and carefully designing an experimental testing scheme.

An important area of research in the field of structural engineering is that of concrete slab behavior. In recent years, the understanding of a phenomenon known as "arching action" has changed the way designers think of concrete bridge decks. Arching action is the formation of compressive and tensile membrane forces after a slab has undergone flexural cracking. This structural action can be visualized as similar to that found in a very flat dome, in which a compression ring forms in the loaded region, and a tension ring forms in the surrounding structure. The principal effect of these membrane forces is to increase the flexural capacity of the cracked slab. This increase in flexural capacity has led to changes in the way engineers design slabs, as exemplified by the "Ontario-type" bridge decks [1,2,3,4,5,6,7,8]. This subject is discussed extensively in Refs. 4 and 6.

Since flexural capacity of a deck is increased by arching action, punching shear can then control the design. However, research pertaining to punching shear in bridge slabs is limited, and research involving fatigue effects on punching shear is even more rare. Consequently, the Texas Department of Transportation initiated a three-year investigation into the effects of fatigue deterioration on the punching shear resistance of highway bridge slabs. A vital aspect of this research project was the development of a relevant, working bridge deck model, and a testing procedure to validate the model analysis.

1.2 Scope and objectives

The general purpose of Texas Department of Transportation Project 3-15D-92/4-1305 is to develop guidelines that will specify the required thickness of bridge decks as a function of various characteristics, such as loading level, wheel spacing, and fatigue history. To determine these guidelines, the fatigue behavior of concrete slabs must be carefully analyzed. This consists mainly of testing slabs in different types of fatigue, and plotting "S-N curves," which display slabs' maximum stress ranges versus the number of fatigue cycles to failure.

The objectives for Project 1305 are as follows:

1) To review past research pertaining to the wheel load, axle width, and axle spacing characteristics of standard and nonstandard loads.

2) To use structural analysis computer programs and engineering models to estimate the stress range experienced by a full-scale cracked bridge deck subjected to a conventional truck loading, and to predict the maximum principal tensile stress in the cracked deck.

3) To design and construct a test setup that will allow for the static and dynamic testing of full-scale bridge decks, including both rolling and pulsating (constant location) loads.

4) To develop S-N curves for both pulsating and rolling fatigue, and to use these curves to determine the effects of rolling versus fixed load applications, and of arching action.

5) To recommend guidelines for specifying the required thickness of bridge deck slabs as a function of traffic characteristics.

The purpose of this report is to describe the development of the experimental program used to research the effects of fatigue on the punching shear capacity of a concrete bridge deck. This development involves the planning of a testing program, the design and construction of a testing apparatus, and the use of the apparatus for the proper testing of representative concrete bridge decks. This report will also include sample results to validate the testing program.

The objectives of this report are as follows:

1) To develop an experimental testing program that, within a reasonable time, adequately shows the effects of fatigue on the punching shear resistance of concrete bridge decks.

2) To develop a testing apparatus on which concrete slabs can be tested in fatigue, both pulsating and rolling.

3) To design the aforementioned setup and slab specimens, construct both setup and specimens, and use both in showing fatigue deterioration of the slabs' capacities.

4) To present an initial sample of experimental test results.

The complete investigation of bridge decks and recommended guidelines will be fully detailed in future reports.

CHAPTER 2
BACKGROUND

2.1 Introduction

This chapter will present an overview of arching action in concrete slabs, a discussion of fatigue, and a review of past research conducted concerning arching action, fatigue effects, and punching shear in concrete slabs. To fully understand the process of developing the experimental tests for this project, one must grasp the theories being tested and comprehend the expected behavior of the test specimens.

2.2 Arching action

When an uncracked bridge deck undergoes loading, it acts primarily as a one-way system, resisting the load with transverse flexure. In-plane action remains insignificant in bridge decks before flexural cracking. However, once the deck cracks near the point of loading and above the supports, it acts as a flat dome. This subject is discussed extensively in Refs. 4 and 6.

This "dome" is defined by a compression zone near the point of load, and a surrounding zone of tension, as shown schematically in Figure 2.1. The compressive membrane forces surrounding the load increase the flexural capacity of the slab. This membrane action exists even if supports are not restrained; the magnitude of such in-plane forces is higher for slabs whose edges are restrained.

Recently, some have attempted to utilize the increased capacity of slabs due to arching action in the design of highway bridge decks. In the mid-1970's, the Ontario Ministry of Transportation and Communications adopted a code that allowed for the empirical design of bridge decks. This empirical design, based on survey data from actual bridge loadings, requires an isotropic reinforcing layout that uses much less steel than current AASHTO design procedures. Much research has been conducted testing this procedure, and many actual bridges have been built using this design method, and have subsequently performed satisfactorily.

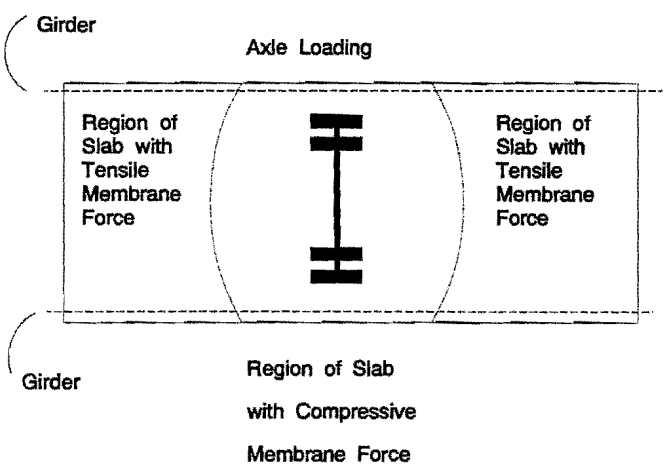

Figure 2.1 Zone of compression balanced by surrounding zone of tension, arching action

Another question about arching action is how its behavior is affected when the load is applied in more than one place. As mentioned before, a point load creates the effect of a flat dome in a concrete slab. However, little is known about how a line load or a group of closely spaced loads might affect this dome-like

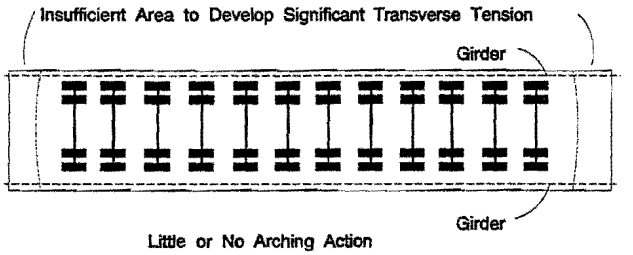

Figure 2.2 Lack of arching action in slab subjected to closely spaced axles

behavior. This is a practical concern in bridges when dealing with long, multi-axle trailers carrying unusually large loads. In the point-load scenario, the "dome" is created by a central compression zone, balanced by a surrounding tension ring. If this tension ring is also loaded, it will go into compression, causing the tension zone to spread toward the supports, as shown in Figure 2.2. This "spreading" of the dome reduces the effectiveness of the arching action.

2.3 Fatigue

Under cyclic stresses, a material's load-carrying capacity can deteriorate — the higher the number of cycles, the greater the deterioration. If a material is subjected to a large number of loading cycles, its ultimate capacity can decrease, even if the level of load is fairly small relative to the ultimate value. This phenomenon, referred to as fatigue deterioration, is of particular concern in the design of highway bridges and bridge decks. These structures are subjected to millions of loading cycles over their design lives, sometimes at very large loads relative to the loads assumed for design purposes.

To predict the reduction in the capacity of a fatigued structure, one must establish a relationship between the relevant stress range and the number of stress cycles. This relationship is typically known as an "S-N curve." An example of an S-N curve is shown in Figure 2.3.

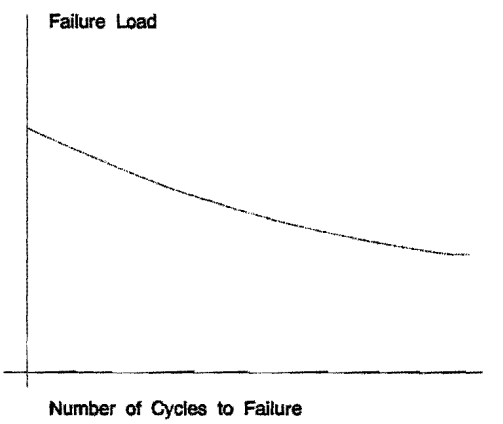

Figure 2.3 Example of an S-N curve

On an S-N curve, the zero-cycle point is merely the static capacity of the slab, and is relatively easy to predict through analysis. However, the rest of the curve is less well known, and finding points through experimental tests is an important goal of this project. For real bridges, fatigue cycles can be estimated as a function of traffic and age, and these experimental S-N curves can then be related, through analytical models, to the reduced capacity of the real bridges.

Two types of fatigue will be studied in this project: pulsating fatigue, which concerns a constant-location, varying-magnitude load; and rolling fatigue, which concerns a constant-magnitude, varying-location load. Separate S-N curves will be developed for each type of fatigue loading.

2.4 Other research

The subjects of arching action in concrete bridge decks and fatigue behavior of concrete slabs have been an important subject in recent structural analysis research. Two important studies that are worth noting and that have influenced this project are a previous University of Texas at Austin study of Ontario-type bridge decks [2,3,4,5,6,7,8], and a project at Case Western Reserve University that examined rolling fatigue of concrete slabs [9,10].

2.4.1 University of Texas at Austin. In the early 1980's, the Texas State Department of Highways and Public Transportation sponsored a study with the Center for Transportation Research at The University of Texas at Austin. The study dealt primarily with the investigation of Ontario-type concrete bridge decks on steel girders. Experiments were performed on a 49-foot-span (14.94-m), full-scale bridge that was a combination of cast-in-place decks and precast, prestressed panels covered with a cast-in-place topping. Both fatigue and static loads were placed on the test bridge.

This study showed that bridge decks designed in accordance with the Ontario Highway Bridge Design provisions performed satisfactorily under AASHTO design loads, even though the decks had about 60 percent of the reinforcement required by the AASHTO code.

A general punching shear model was used to predict the deck's capacity and accurately predicted the experimental punching shear capacity. Finite element analyses were also performed and agreed closely with the experimental results. The ACI and AASHTO formulas for punching shear proved to be fairly conservative.

These results from the Ontario-type bridge deck experiments proved two main points that are important to current research. Firstly, the adequate performance of the Ontario-type decks, with lower reinforcement ratios than those required by AASHTO, showed that arching action is indeed beneficial and can be utilized in the design of the flexural capacity of concrete slabs. The second important result is that, because of this increased flexural capacity due to arching action, punching shear will govern in the failure of concrete bridge decks.

2.4.2 Case Western Reserve University. More recently than the University of Texas work, Perdikaris and others studied the effects of pulsating and moving loads on concrete bridge decks designed with both orthotropic reinforcement (as per AASHTO), and isotropic reinforcement (as per Ontario-type decks) [9,10]. Experiments were performed on 1/6.6-scale model decks, with thicknesses of 1.25 inches (31.75 mm), supported on steel girders.

The research at Case Western Reserve University concluded that the fatigue life of decks designed by the Ontario Code (with isotropic reinforcement) is about 20 times the fatigue life of decks designed by the AASHTO provisions (with orthotropic reinforcement). Also, the factor of safety for static ultimate failure is about 14 for isotropically-reinforced decks, and 23 for orthotropically-reinforced decks.

Other results from this research were more disconcerting. When the slabs were subjected to moving loads, extensive grid-like cracking patterns were observed, producing "alligator-skin" surfaces

on the models. This widely distributed cracking may be due to any number of factors, but certainly one must consider the scaling effects of the 1/6.6-scale model, as well as the effects of the test setup, which consisted of a moving steel wheel coated with a layer of hard polyurethane.

It is the goal of the current research to further study the effects of pulsating and moving loads on concrete bridge decks, using full-scale models and realistic loading methods.

CHAPTER 3
ANALYTICAL BASIS — SLAB MODELS

3.1 Introduction

Before any experimentation can be performed, a researcher must understand the basic principles that govern the behavior of the laboratory specimen. Ideally, one would want analytical models that simulate the exact behavior of the real subject.

In this project, several slab models were analyzed using the finite element method, whereby a structural system is discretized into a continuous mesh of smaller elements, each a separate member in the structure's stiffness matrix. Then, the structural elements are analyzed using basic structural theory.

Of the models studied, two were most important: one model represented a typical highway bridge, with a full-length, 50-foot (15.24-m) span and realistic dimensions; and the second model depicted the actual experimental specimen to be tested. The analyses of these models and their relationship to each other were crucial in the design of the specimens and of the testing program.

3.2 Complete bridge model

In order to assure that the behavior of the chosen experimental specimen could be related to a real highway bridge deck, a finite element model of a full-size bridge had to be analyzed. A typical highway bridge with typical AASHTO truck loading patterns was chosen. This prototype was a three-girder, 50 foot-span (15.24-m) bridge with a 7-foot (2.13-m) girder spacing and a 3-foot-3-inch (.99-m) overhang on each side. The bridge consisted of a 7½ inch-thick (191-mm) concrete deck on top of three W36x150 steel beams.

The finite element model of this full-size bridge included two types of elements: the concrete deck was modeled using 8-node isoparametric brick elements, while the steel girders were modeled using three-dimensional, 2-node beam-column elements. The brick, or "solid," elements have three displacement degrees of freedom, while the beam-column, or "frame," elements have three displacement and three rotational degrees of freedom.

In order to reduce computational time and effort, a plane of symmetry was cut along the longitudinal axis of the center girder, and half of the bridge was modeled. This was allowed due to the symmetry of the bridge's geometry, as well as the symmetry of the loading pattern. The modeled half of the deck consisted of 238 solid elements, and the two girders consisted of 17 frame elements each. Figure 3.1 shows the finite element mesh for this full-size bridge model.

The loading pattern for the full-size bridge was based on a typical AASHTO HS20-44 truck loading patterns, with three pairs of loading points (three pairs of tire groups), representing a truck and

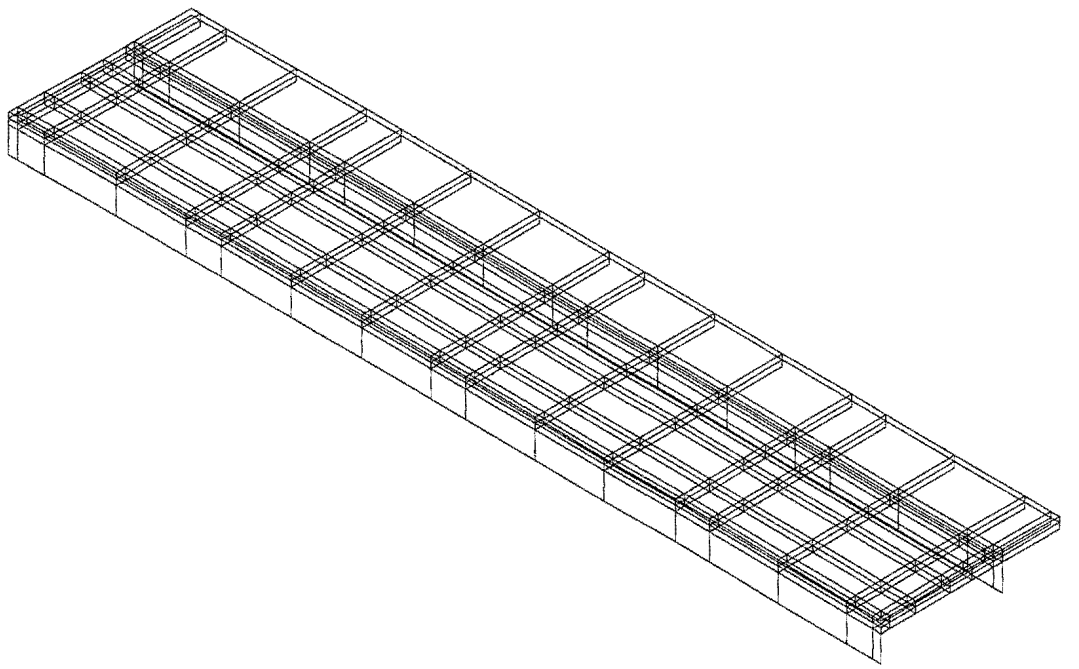

Figure 3.1 Finite element model for full-size, 50 foot-span (15.24-m) highway bridge. Only half of the bridge is modeled due to symmetry

trailer. A total load of six times the AASHTO design load (6 times 72 kips (320.4 kN)) was placed on the bridge model and analyzed as described in Section 3.4. The load magnitude was selected to represent an extreme overload that would be useful in examining the low-cycle end of the S-N curve.

3.3 Experimental specimen model

The main reason for modeling a full-size bridge system was to verify that the chosen experimental specimen would behave in a manner similar to a "real-world" bridge deck. For this verification, another finite element model was needed, this time modeling the specimen to be used in the laboratory tests.

Initially, the size of the specimen was dependent on typical highway bridge girder spacing. Also, given a certain size loading footprint (close in dimensions to an actual pair of tires), it was important to ensure that a punching shear failure mechanism had space in which to occur. In other words, there had to be room for a truncated cone to form within the space defined by the supports.

Given the above constraints, the slab specimens were designed to be 6 feet (1.83 m) wide (typical girder spacing), 7 feet (2.13 m) long (in the direction of travel), and 7½ inches (191 mm) thick (typical cast-in-place deck thickness). This specimen was modeled using a finite element mesh consisting of 8-node solid elements similar to those used in the deck of the full-size model described above. A total of 1,344 solid elements was used to model the experimental slab. Again, only half the slab was modeled due to symmetry. The specimen model is shown in Figure 3.2.

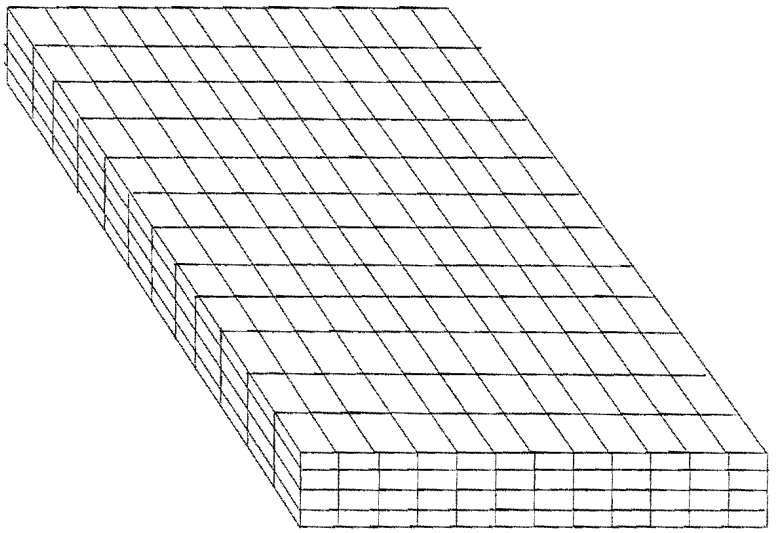

Figure 3.2 Finite element model for experimental specimen tested in laboratory. Only half of the slab is modeled due to symmetry

The finite element model was important for analytical verification of arching action. One could observe the stress ranges at critical sections in the slab, and compare these with stress ranges from the full-size bridge model.

The specimen model was also important in deciding, for the rolling fatigue tests, how much movement would be necessary to produce the desired stress ranges within the slabs. This is discussed in more detail in Sections 3.4 and 3.5.

3.4 Methods of analysis

An analysis is only as good as its assumptions. To fully describe the methods of analyses used for the full-size bridge model and the specimen model, it is necessary to discuss the assumptions and theories used in both analytical models. It is also necessary to discuss any assumptions inherent in any analytical tools used — in this case, the finite element models and program.

All finite element analyses on this project were performed using SAP90, a widely available microcomputer structural analysis program [11]. It allows for many different types of elements, but for the models discussed above, only the 8-node brick element ("solid"-type) and the 2-node beam-column element ("frame"-type) were used. The solid element is limited somewhat in that it models only displacement degrees of freedom, and not rotational. It is an isoparametric, three-dimensional element that performs satisfactorily if used in a fairly refined mesh [11,12]. While the frame element has

displacement and rotational degrees of freedom, for this project these were used only to model the steel girders in the full-size bridge.

One drawback of the finite element program used on this project is that it conducts only elastic analyses of structures. This is especially a problem when studying arching action effects, since concrete must crack for membrane forces to be present. Ordinary elastic analysis does not take into account the cracking of concrete, and the subsequent stressing of the reinforcing steel.

To avoid the inaccuracies of a strictly elastic analysis, more complicated procedures were used. In order to obtain a pseudo-nonlinear response from the models, a sequential linear analysis was performed. To do this, a small load was applied to the models and incremented until the stress in any concrete element reached the cracking stress for concrete.

The model was then modified to take into account the cracked elements. This was accomplished through a method known as smeared crack modeling, which assumes that an entire element has the same reduced stiffness as long as any stress in that element exceeds the cracking stress for concrete. Therefore, the stiffness of these elements was set to zero in the direction perpendicular to the crack's orientation.

The sequential linear analysis was then continued by applying an incremental load until more elements reached the cracking criterion. Those elements, in turn, were modified with a smeared cracking stiffness, and the process was repeated. A sample load-deflection curve from a sequential linear analysis is shown in Figure 3.3. It can be seen that the structure's total stiffness will reduce as more elements are cracked. This gives the dotted envelope curve a nonlinear shape, with a decreasing slope.

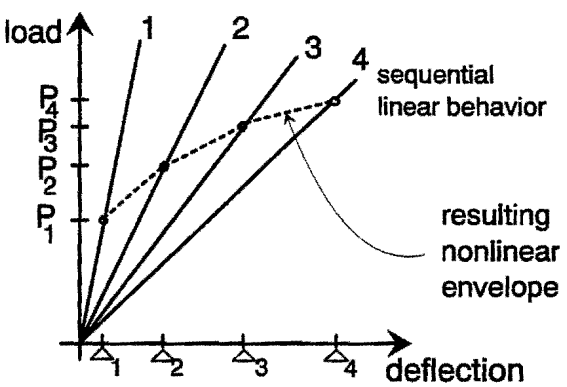

Figure 3.3 Example of load-deflection curve using sequential linear analysis

3.4.1 Full-size bridge analysis. As discussed above, the full-size bridge model represented half of a three-girder bridge. The girders were modeled with frame elements, and were supported at the ends of the 50-foot (15.24-m) span. The girder elements were given all the properties of steel W36x150 rolled shapes. Because of symmetry, the center girder was actually half an actual beam (cut through its longitudinal axis); therefore, it was given only half the stiffness of a full W36x150.

For the loading of the full bridge model, it was important to try to imitate the actual loads for which a bridge is designed. Therefore, the loading pattern modeled one design load, as presented in the AASHTO specifications for highway bridges. The HS20-44 truck and trailer loads and load configuration are shown in Figure 3.4. The magnitude of loading applied to the analytical model was actually six times higher than the AASHTO loads. This was done to create full cracking and arching action effects in the bridge deck, and to be able to compare the full bridge results with those of the experimental model,

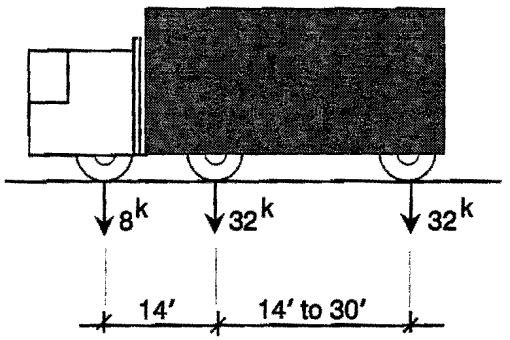

Figure 3.4 AASHTO design loads for standard HS20-44 truck

which would be loaded to ultimate strength. Therefore, the maximum wheel load on the bridge (192 kips, 854.4 kN) was close to the load applied to the smaller specimen model (200 kips, 890 kN). The loading pattern for the full-size bridge model is shown in Figure 3.5.

The next step was to load the full-size bridge model incrementally, as described above in the discussion of sequential linear analyses. Once the bridge was fully loaded and all elements above cracking stresses were modeled as cracked elements, stresses in the slab could be displayed both numerically and graphically, and compared with stresses from the specimen model.

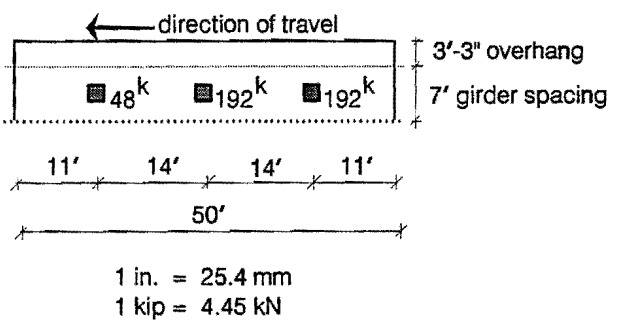

Figure 3.5 Plan view of loading pattern for full-size bridge model

3.4.2 Experimental specimen analysis. The finite element model representing the experimental slab specimen was analyzed in much the same way as the complete bridge model. Sequential linear analysis was used, incrementally loading the slab and modeling cracked elements as they reached a critical stress. This allowed the development of a pseudo-nonlinear load-displacement curve, as was done for the full-size model.

The loading pattern used for the specimen model, however, was different from that used for the bridge model. It was necessary to try to model the load exactly as it would be applied to the experimental specimen. The loading pattern for the specimen model is shown in Figure 3.6.

3.5 Relationship between analytical models

Of primary interest in the analytical models were the stresses that the arching action, or membrane forces, would produce within the models when fully loaded and cracked, where "fully loaded" refers to the loading that produces a punching shear failure in the experimental specimen.

Two important characteristics were studied in the finite element model comparison. First, the models were analyzed for general arching action behavior, observing in-plane stresses, membrane forces,

and support reactions. In both models, the expected arrangement of a central compression area surrounded by a tension ring was found. Elemental stress analysis, as well as graphical stress contour maps, confirmed general arching action behavior. Also, the models confirmed that arching action is even present in slabs that do not have lateral-resistant supports.

Another important factor needed from the experimental specimen model pertained to the rolling fatigue test. It was necessary to know how much lateral movement of the load was needed to produce the desired stress ranges in the specimen. To accomplish this, the structure was analyzed many times, each time with the load at a slightly different position. Then, the diagonal tension stress along the assumed failure plane was noted. The assumed punching shear failure surface, verified in previous studies [4], was a 38-degree plane representing a truncated cone, as shown in Figure 3.7.

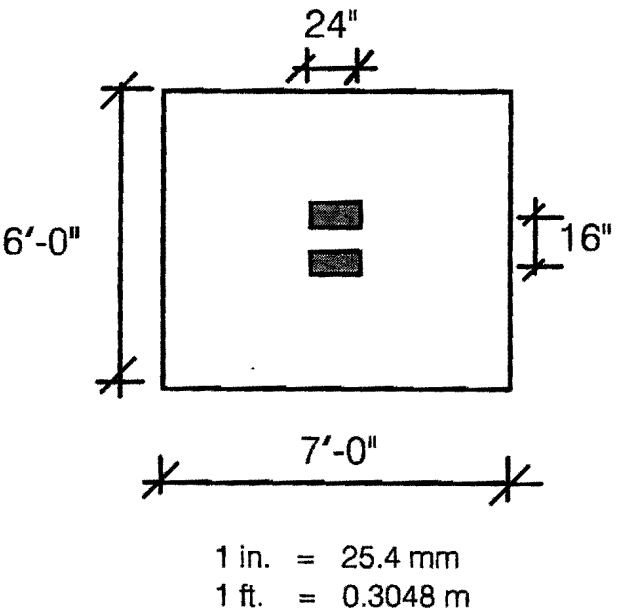

Figure 3.6 Plan view of loading pattern for specimen model

From this incremental analysis, it was possible to find the minimum movement of the load necessary for the maximum tensile stress perpendicular to the failure plane to go from the cracking tensile strength to a compressive stress. This assured that when the rolling load was at the extreme end of its travel, the failure surface on the other end of the travel would not experience the detrimental effect of the load. The necessary travel was found to be 18 inches (457.2 mm).

In summary, two important facts were obtained from the finite element analyses of the full-size bridge model and the experimental specimen model:

1) Arching action in cracked slabs exists and is easily observable in analytical models, even those without lateral restraint of supports. Also, although the full-size bridge model was loaded and supported differently than the experimental specimen model, both models exhibited similar arching action behavior. This behavior consisted of the formation of a compression zone in the loaded region, surrounded by a tension ring. Stress contours for both models are

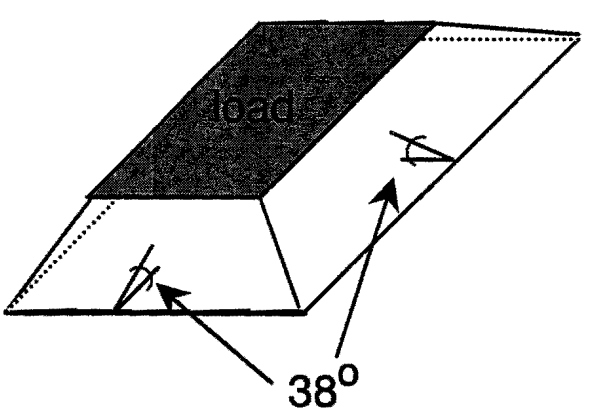

Figure 3.7 Assumed failure surface of a general punching shear model

shown in Figures 3.8 and 3.9. It is noted that the stress contours of Figure 3.9, obtained from actual analyses, are quite similar to the single-axle contours of Figure 2.1. Also, the multiple-axle contours of Figure 3.8 are quite similar to those shown qualitatively in Figure 2.2.

2) For the rolling fatigue tests, the load needs to move a total of only 18 inches (457.2 mm) (9 inches (228.6 mm) on either side of the slab's centerline) for the failure surface to experience the full stress range of tension to compression. This movement will produce the stress range necessary to cause full fatigue failure.

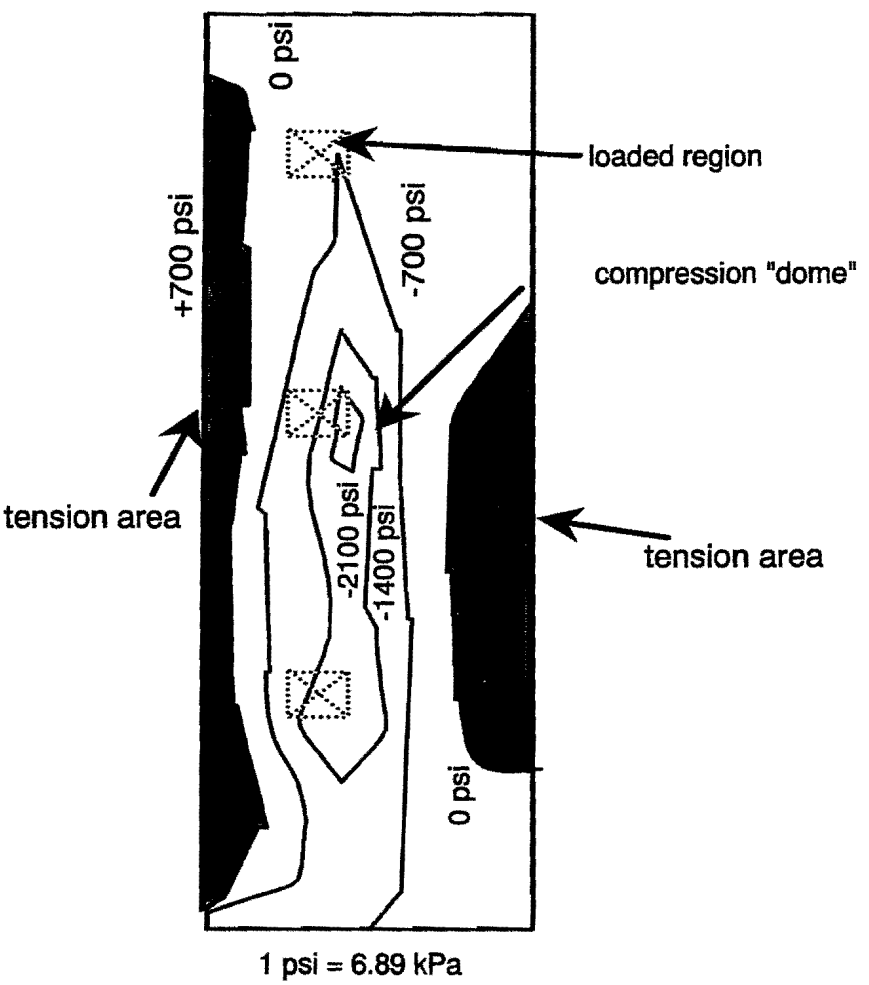

Figure 3.8 Stress contours from finite element analysis of full-size bridge model, showing the effects of arching action (shaded regions denote areas of tensile stresses)

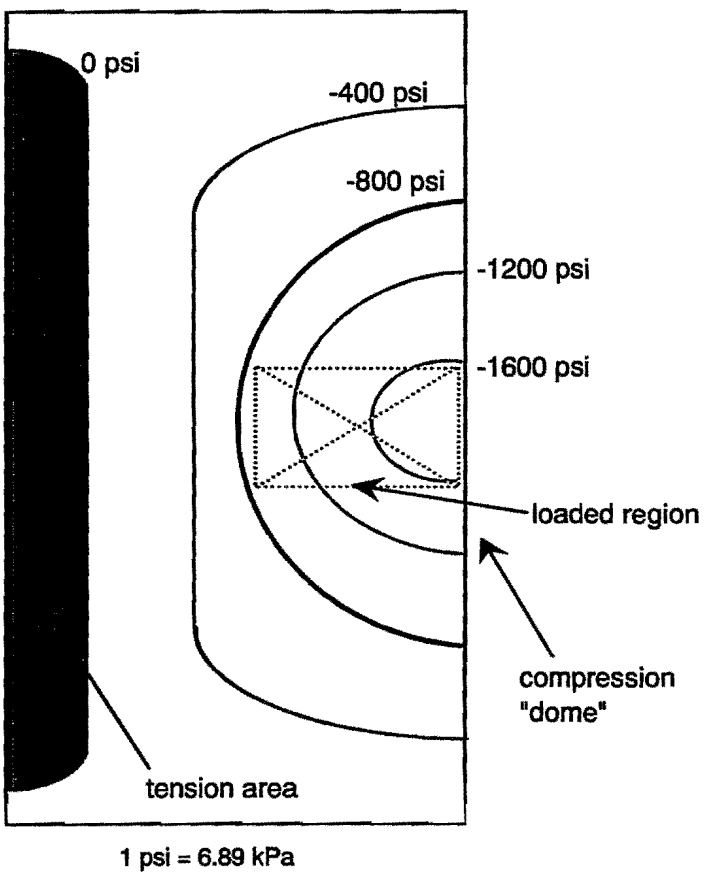

Figure 3.9 Stress contours from finite element analysis of experimental specimen model, showing the effects of arching action (shaded regions denote areas of tensile stresses)

CHAPTER 4
DEVELOPMENT OF TEST SETUP

4.1 Introduction

The following chapter describes the design and implementation of the experimental testing program, including test specimens, testing frame, instrumentation, loading, and data acquisition during testing.

4.2 Test specimens

4.2.1 Scale and size. An important consideration in any experimental research is how well the subject being tested represents the actual "real-world" object. In this case, knowledge of actual highway bridge decks is desired, and, therefore, actual bridges would be the ideal testing specimens. Of course, this would be enormously expensive, so one must try to simulate actual bridge behavior within the controlled environment of the laboratory, preferably at a reasonable cost and time.

For this research, it was deemed desirable to test full-scale concrete bridge deck specimens in order to eliminate any scale effects produced by using small specimens, such as extensive cracking, lack of reinforcement development, etc. To create a full-scale slab, a specimen thickness of 7.5 to 9 inches (191 to 229 mm) was decided upon, since this was the average thickness of most cast-in-place bridge decks in Texas.

The next consideration was how large to make the specimens, or, in other words, how much of the loaded region of the bridge needed to be represented. The width of the specimens was determined from average girder spans of bridges in Texas, about 6 to 8 feet (1.83 to 2.44 m). The length of the specimens was more difficult to determine, and depended directly on how much of the slab was needed to represent a loaded region on an actual bridge. Actual bridge behavior was determined through the use of various finite element models, as described in Chapter 3. The length of the slabs was controlled by the test involving rolling fatigue, and how much of the slab was necessary to completely surround the compression "dome" created by the arching action when the rolling load was at its outermost point of application.

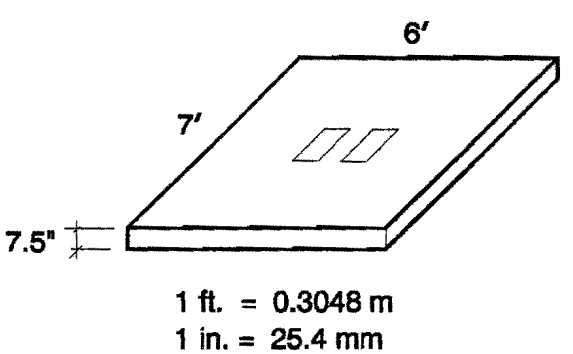

Figure 4.1 Dimensions of full-scale slab model

The dimensions of the initial slabs were 6 feet (1.83 m) wide, 7 feet (2.13 m) long (direction of travel), and 7.5 inches (191 mm) thick, as shown in Figure 4.1.

4.2.2 Reinforcement. Since this research is primarily concerned with punching shear and its characteristics under fatigue loading, it was necessary to design the specimens in such a way that a general punching shear failure occurred, as opposed to a flexural, bond and development, or direct shear failure.

In order to guard against a flexural failure, the specimens that would be loaded in excess of AASHTO loads were designed with higher than normal flexural reinforcement, about three times the usual bottom steel used in highway bridges. The typical bottom reinforcement for the most heavily reinforced slabs was two #6 bars (bundled) at 12 inches (304.8 mm) on center, in both directions. Those slabs that will be loaded at lower levels will have much less reinforcement, corresponding to percentages typically used in design.

Another undesirable mode of failure is a bond and development failure of the reinforcement. This was an important concern since the experimental models were only segments of a bridge slab, without the continuous ends that would normally be found in actual bridges. Without continuous slabs over the supports to provide sufficient development length for the flexural reinforcement, another method of providing a development length had to be found. The best method was discovered to be 180-degree hooks on the bottom reinforcement, in both directions, in order to prevent a bar pull-out failure over the supports.

To prevent a direct shear failure, it was required that the slabs be supported inside of the hook plane. This prevented the side cover from shearing off due to concentrated loads on the edge of the slab.

Grade 60 #4, #5, and #6 (12-mm, 16-mm, and 19-mm) reinforcing bars were used in the specimens.

4.3 Testing frame

Since this research project was attempting to test full-scale bridge decks, very large loads would be necessary to fail the specimens in the desired fashion. To place these large loads on the slabs, a very stiff and strong steel frame was necessary.

An important consideration in the test frame design was also fatigue. Because the specifications called for moving and rolling fatigue tests involving large loads and many cycles, it was crucial that the tests would fatigue and fail the slabs, not the testing frame.

Another concern with the fatigue tests was time. Many of the fatigue tests would require over a million cycles and, therefore, one test might monopolize the testing frame for several weeks. Therefore, to increase the efficiency of the testing, a frame that allowed multiple, simultaneous tests was designed, as shown in Figure 4.2. The test setup consists of three bays and is capable of testing three slabs that are 7 feet (2.13 m) long and of variable width and thickness.

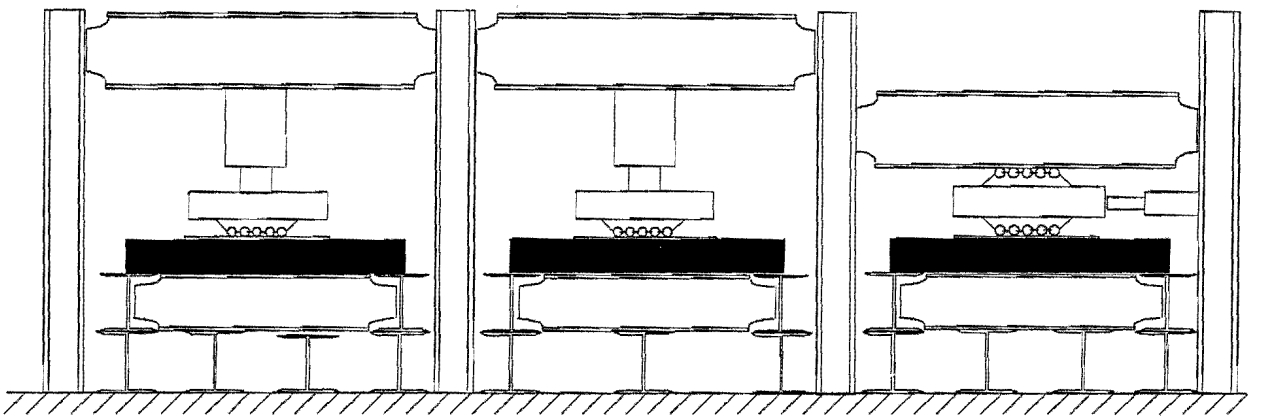

Figure 4.2 Steel testing frame showing two pulsating fatigue test and one rolling fatigue test

The steel frame consisted of A36 rolled steel shapes, primarily wide-flange (W12's and W14's) for the girders and beams, and channel sections (C12's) for the columns. Angles and A325 bolts were used for connections. Welds were avoided wherever possible, due to the concern of the fatigue performance of welded connections.

4.4 Instrumentation

For monitoring behavior within the initial set of three slabs, a total of 15 strain gages measured strain and, therefore, stress, in both the steel and concrete. Ten gages were applied to both the top and the bottom steel, in both directions, prior to the placement of the concrete. After removal of the wood forms and prior to testing, five gages were applied to the underside of the hardened concrete, directly beneath the location of the steel gages.

To monitor general slab displacements during loading, three linear potentiometers were connected to the slab. One was placed at the center-point of the slab to monitor downward deflection, while the other two were placed on the edges of the slab to monitor any uplift or rotational displacement of the slab over the supports. Also, analog dial gages were placed at various locations to monitor frame deflection and frame-slab interaction.

Loads were monitored with both a load cell and a pressure transducer, and their readings were compared for accuracy.

4.5 Loads

In this project, there were three main load cases: 1) static loading, 2) pulsating fatigue (fixed location - varying magnitude), and 3) rolling fatigue (fixed magnitude - varying location). Each load case required different frame configurations and different loading methods.

The static load tests are primarily used for finding the ultimate punching shear strength of the slabs. They are the "zero-cycle" point on the S-N curves. The load is monotonic, with no fatigue loading. For the experiment, the load was applied through a single 400- or 500-ton (3560- or 4450-kN) hydraulic ram, with hydraulic fluid applied through a hand pump.

The method of applying the load from the ram to the slab was very important. The most desirable method would be through an actual truck tire, in order to simulate the truck "footprint" that an actual bridge would experience. However, due to the extremely large loads that these full-scale slabs would encounter (about 200 kips) (890 kN), a real, pneumatic tire would be impractical. Therefore, a hard roller or castor was needed, but undesirable due to the harsh localized effects such hard objects would have on the concrete surface. The solution was to use a steel roller skid, but with a thin neoprene pad covering the loaded surface. This would allow extremely large, movable loads while reducing any localized damages caused by the steel rollers.

For the pulsating fatigue loading, the testing setup was identical to the static test, except the hydraulic fluid was supplied through a electric pump connected to a closed-loop servo-controller.

For the rolling fatigue loading, the testing frame was modified from the setup described above (see Figure 4.2). The load on the slab was applied through a "clamping" of the top girder to the bottom beams. This clamping was applied through four rams, one at each corner of the top girder, and produced a compression in the roller skids at the center of the slab. These skids had rollers on both top and bottom, allowing them to be moved back and forth by a horizontal ram. The moving range was approximately 18 inches (457.2 mm). The vertical load was then held constant during the test, while the horizontal ram was controlled by a closed-loop servo-controller.

4.6 Data acquisition

In order to monitor the 15 strain gages, two displacement potentiometers, one load cell, and one pressure transducer, a computerized data acquisition system was used. The system consisted of a Hewlett-Packard scanner, a microcomputer, voltage suppliers, and storage devices. Readings were taken at necessary intervals, depending on the type of test, magnitude of loading, and number of cycles.

CHAPTER 5
TESTING PROCEDURE

5.1 Introduction

In this research, three different types of tests were performed. Some slabs were tested under a fixed, static load in order to verify analytical models used to predict ultimate punching shear capacity. Other slabs were tested under a pulsating fatigue load, in which the load was applied at a fixed point, and varied in magnitude with time. The third type of test was a rolling fatigue test of slabs, where a fixed vertical load was applied to the slab through a set of rollers, and then moved back and forth along the slab.

5.2 Static tests

The first experiments performed for this project were static load tests, which were used to find the ultimate punching shear capacities of the slab specimens. These static tests also verified both the finite element model of the specimen, and also the general punching shear model used to predict the ultimate punching shear capacity. This general model assumed a truncated cone with a failure plane of 38 degrees to the horizontal, as discussed in Chapter 3.

The static tests were performed using the testing configuration shown in Figure 5.1. The testing frame allowed for the simultaneous testing of three slabs, but only one is shown in the figure.

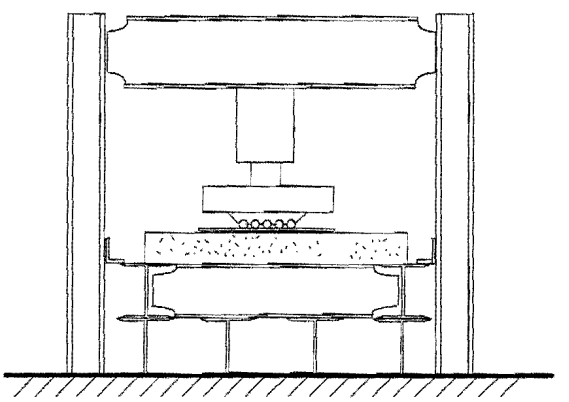

Figure 5.1 Setup for static tests of slab specimens

The frame consisted of columns made up of 4 channel sections, and a top girder system consisting of two W14 rolled sections and two one-inch-thick (25.4-mm) plates. Each side of the slab was supported on a W12 section, and these four beams, in turn, rested on four more W12's oriented transverse to the slab. The four bottom beams' primary purpose was to elevate the slab and its supports, in order to provide access to the underside of the slab. This was necessary in order to apply external gages, as well as to observe cracking patterns during testing.

Attached to the top girder was a 400-ton (3560-kN) capacity hydraulic ram. For the static tests, load was applied through the ram by applying a hydraulic pressure with a hand pump. The load was applied to the slab through two heavy-duty roller skids attached to the web of a W27 lying on its side. Between the steel roller skids and the slab was a half-inch-thick (12.7-mm) sheet of neoprene, which

provided some protection of the slab from localized damage, and simulated the contact between rubber tires and concrete.

The load was monitored by a load cell in contact with the ram, as well as by a pressure transducer attached to the hand pump. Displacement of the slab was recorded using a series of strategically placed linear potentiometer. Strains in both the concrete and the reinforcing steel were monitored using electrical-resistance strain gages. All information was recorded using a Hewlett-Packard scanner and a microcomputer.

During each static test, the load was applied monotonically to the center-point of the slab until a punching shear failure occurred. The punching shear capacity for the static tests was then considered the "zero-cycle" ordinate on the S-N curves, whereas the pulsating fatigue tests would supply other capacities at different numbers of loading cycles. Also, for the static tests, load-displacement curves could be created, showing stiffness changes in the cracking slab.

5.3 Pulsating fatigue tests

The first fatigue tests performed on slab specimens were referred to as "pulsating" fatigue; in these, the applied load varied in magnitude but stayed at a constant location. These tests were intended to study how various levels of loading and numbers of cycles would affect the punching shear capacities of the slabs. This fatigue deterioration would be monitored using S-N curves, plotting failing stress ranges versus number of cycles to failure.

The test setup used for the pulsating tests was very similar to that used for the static tests (see Figure 5.1), the main difference involving how the loading was controlled. For the fatigue test, pressure was applied to the 400-ton (3560-kN) ram using an electric pump. The flow of the pump was controlled by an MTS servo-controller which, in turn, regulated a servo-valve and line tamer. The controller could monitor minimum and maximum loads, and count the number of loading cycles applied to the slab. The controller also checked for any large variations in load, and could therefore shut the system down in case of failure or error. The hydraulic system for two simultaneous pulsating fatigue tests is shown in Figure 5.2.

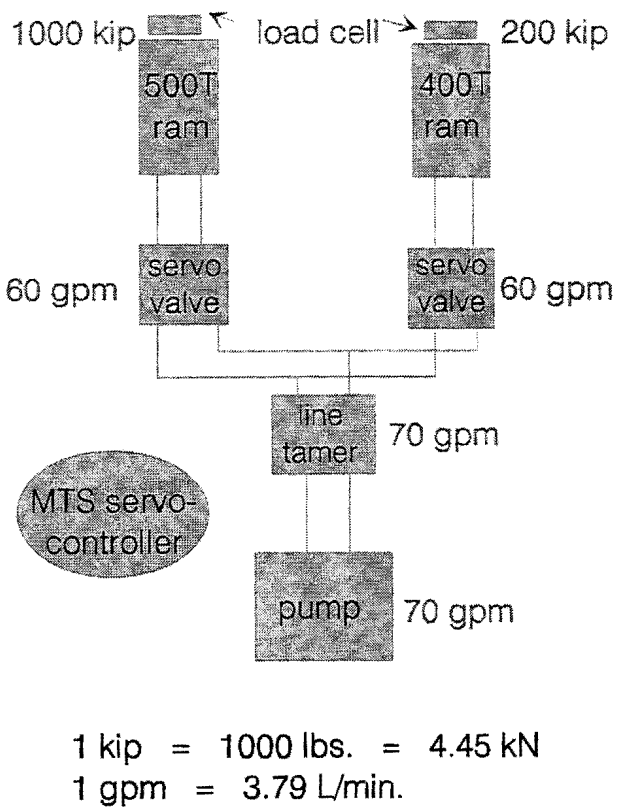

Figure 5.2 Schematic of hydraulic system for two simultaneous pulsating fatigue tests

Because these tests dealt with such large loads, the rate of loading was dependent on how quickly the large amounts of hydraulic oil could be pumped in and out of the ram. Special modifications to the ram, namely the enlargement of the input and output ports, increased the flow rate and allowed more cycles and higher loads in a given period of time.

Each test was conducted until a fatigue failure occurred. The load and number of cycles were then plotted as a data point on an S-N curve. Also, slab displacement, as well as steel and concrete strain, could be monitored periodically during the fatigue loading.

5.4 Rolling fatigue tests

The pulsating fatigue tests described above have traditionally been the preferred method of researching fatigue effects in slabs. However, some concern has been expressed about whether such tests completely duplicate the conditions placed on highway bridge decks. Actual bridges, after all, do not experience such pulsating, stationary loads. Real loadings involve loads at service levels (or slightly higher), applied by rolling vehicles. The effect of this rolling motion on the fatigue deterioration of bridge decks could be substantial, but still remains largely unknown.

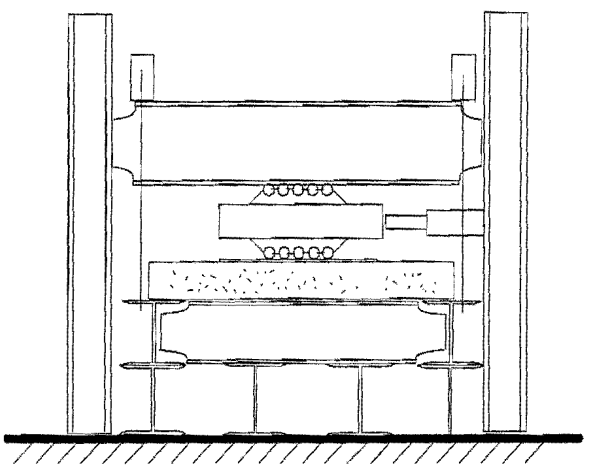

Figure 5.3 Setup for rolling fatigue tests of slab specimens

The main reason that research on rolling fatigue has been rare is probably the great difficulty such experiments can cause. Experimentally, moving loads large enough to fail concrete slabs, especially full-scale slabs, is quite a task.

In this project, the test setup used for rolling fatigue tests resembled the setup used in the pulsating tests, with a few modifications. The rolling fatigue setup is shown in Figure 5.3. The basic frame for this test is very similar to the one used in the pulsating tests (see Figure 5.1). In fact, the only change in the frame involves moving down the top girder until it rests on the loading apparatus, which now consists of four roller skids — two on the bottom and two on the top.

The top girder is then loaded downward by rams on top of the girder. The rams apply the load through a series of rods connecting the rams to the bottom beams that the slab is resting upon. This produces a compressive load through the roller skids, which load the slab with a footprint caused by the two skid treads. Like the other tests, a half-inch-thick (12.7-mm) sheet of neoprene was used to protect the concrete from any wear caused by the steel skids. The neoprene was also covered by a thin steel sheet to prevent cutting.

After the initial load is applied using the top rams, the rams are closed off, maintaining the load in the vertical rods. Then, to obtain rolling action, the skate is rolled back and forth with a horizontal ram connected to the frame columns. As mentioned in previous chapters, the total moving range was 18 inches (457.2 mm). For fatigue loading, the horizontal ram was connected to a servo-controller and controlled by a displacement function. The number of rolling cycles was then monitored in the same way that the pulsating cycles were, as described in the preceding section.

For each test, failure load and number of rolling cycles were plotted on S-N curves. Data points from the rolling tests were then compared with those from the pulsating tests.

CHAPTER 6
SAMPLE TEST RESULTS

6.1 Static test results

The first priority in the experimental schedule was to obtain data for a static load test. It was desirable to have a slab loaded monotonically to failure in order to obtain information regarding ultimate punching shear strength, load-deflection behavior, and assurance in the expected mode of failure. This initial ultimate strength test would also ensure the performance of the testing frame at its highest expected loading, as well as point out any deficiencies in the test procedure in general. Any problems encountered and solved in the static tests would allow for more efficient fatigue testing later in the project.

The first static test was performed on a 6-foot (1.83-m) by 7-foot (2.13-m) by 7.5-inch (191-mm), cast-in-place concrete slab. The 28-day concrete strength was about 6000 psi (41.3 MPa). The slab was over-reinforced in flexure, as described in Chapter 3. The load-deflection behavior of this first slab is shown in Figure 6.1.

The load-deflection curve shows more than one loading/unloading cycle was actually placed on the first specimen. The first cycle placed about 50 kips (222.5 kN) on the slab (about 30% of the expected ultimate), and then unloaded due to equipment malfunction.

The second loading cycle placed on the slab reached a maximum load of 110 kips (489.5 kN). At this loading, the specimen experienced a local support failure along one of the longer edges. The failure was examined and determined to be only a local problem in which the side cover partially sheared off. The edge supports were moved in about 5 inches (127 mm), and the slab was reloaded, this time

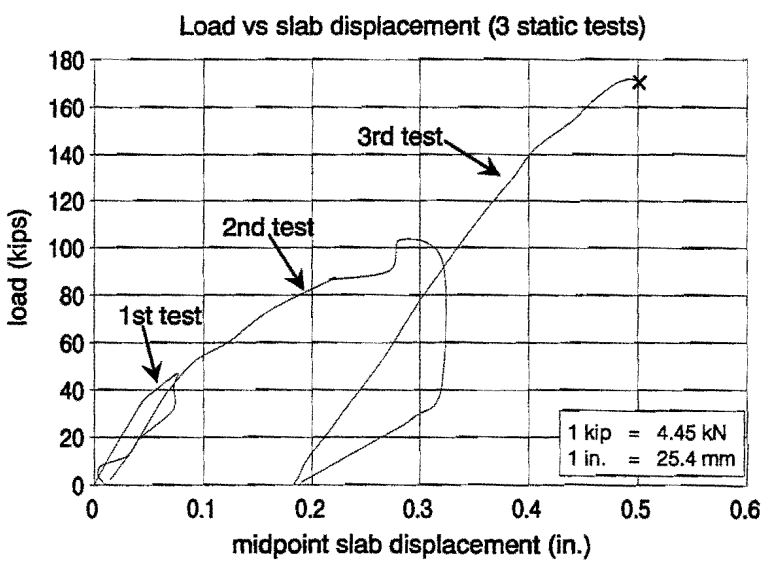

Figure 6.1 Load-deflection curve of first statically loaded slab specimen. Graph shows two initial loading/unloading cycles

to a punching shear failure. As shown in Figure 6.1, the ultimate load placed on the slab was 175 kips (779 kN), which was only about 1 percent higher than the strength predicted by the truncated-cone punching shear theory.

The slab specimen was tested under deflection control: loading was applied to the slab through a controlled extension of the ram piston. Load was applied in approximately 10-kip (44.5-kN) increments, until failure occurred at 175 kips (779-kN).

One observation during testing was the sudden mode of failure. This was expected and is typical of a concrete shear failure. The slab produced a loud "thud" at the ultimate load, and exhibited an immediate drop in load-carrying capacity. The slab continued to be loaded, deflecting large amounts with no increase in load. This increased deflection is not shown in Figure 6.1 due to the loss of the linear potentiometer from spalling of the slab's top surface. The extended deflection was monitored, however, using a dial gage.

The deflection graphed in Figure 6.1 is the midpoint deflection of the specimen, relative to the longitudinal ends of the slab. This was accomplished by attaching three linear potentiometers to the slab: one in the middle, and two on each longitudinal edge. The average of the two edge displacements was subtracted from the midspan displacement. This relative midpoint deflection was obtained in order to isolate the slab behavior itself, and to eliminate the effects of any frame deflection or support uplift.

From observance of the cracking pattern, it was decided that the slab did indeed fail by punching shear. The observed cracking pattern of the slab, on both the top and underside of the specimen, is shown in Figure 6.2. The top of the slab cracked in a square pattern immediately adjacent to the loading footprint. The underside of the slab cracked near the supports, suggesting a very shallow failure plane, about 20 degrees as opposed to the assumed 38 degrees. This

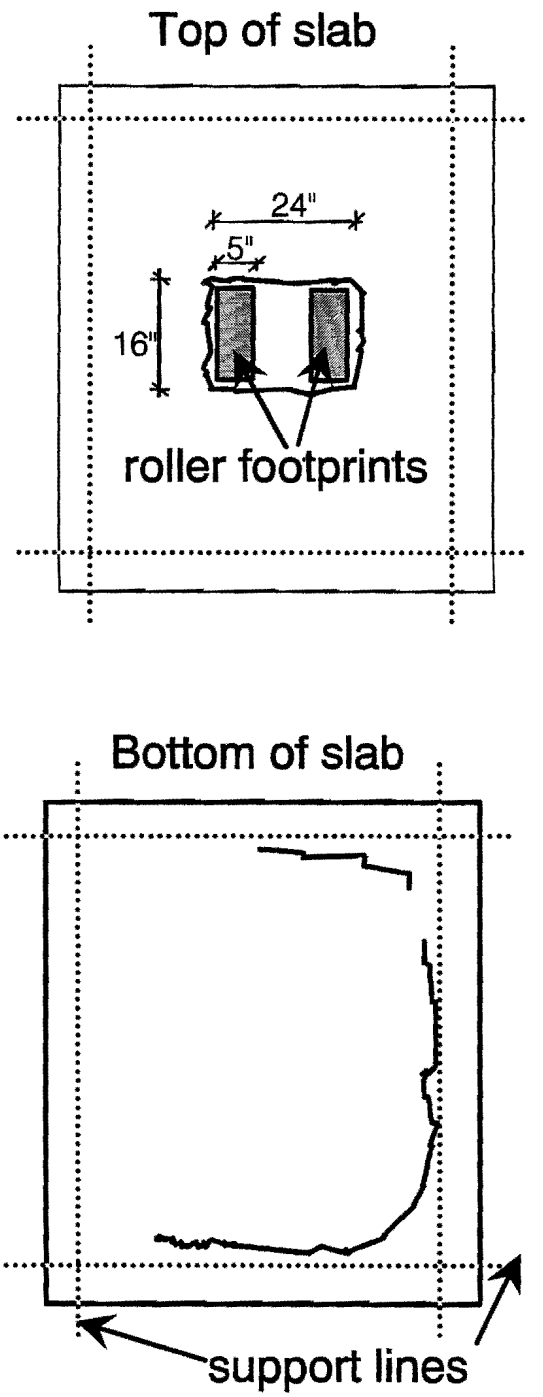

Figure 6.2 Plan view of top and bottom of slab, showing cracking patterns after punching shear failure

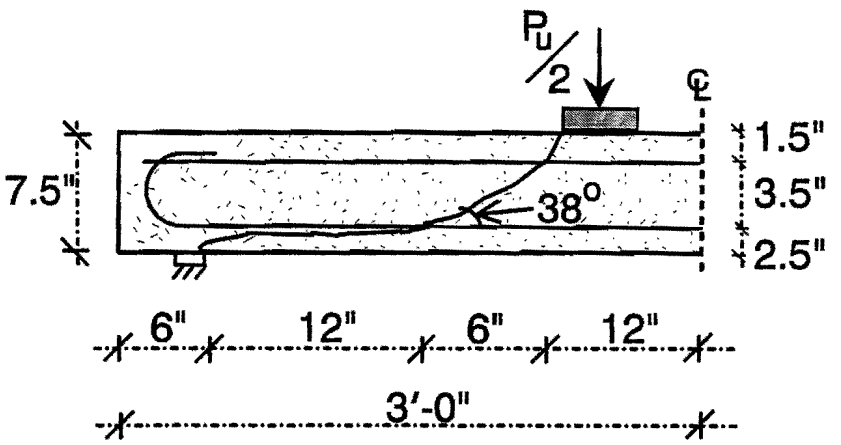

1 in. = 25.4 mm
1 ft. = 305 mm

Figure 6.3 Cross-section of static load test specimen showing observed punching shear failure

cracking is deceiving, however, since the actual crack through the slab was much steeper, and then became shallower as it reached the slab's bottom cover. This behavior was evidenced by stripping off the bottom cover after testing. Figure 6.3 shows the observed punching shear crack in the static test specimen.

Other data collected during the static testing of the slab included concrete strain from external strain gages, and reinforcing steel strain from internal strain gages. The five concrete gages were useful in early testing, but were damaged after the slab was extensively cracked.

Of the ten internal steel strain gages, two were damaged during placement of the fresh concrete. Most of the remaining gages remained useful up to punching shear failure of the slab. Figure 6.4 contains two plots of load versus steel strain. The first plot shows strain in the top layer of reinforcing steel, while the second plot pertains to the bottom layer of steel. As expected, all of the bottom steel experienced higher tensile strains than the top steel. The plots also show that, for both layers, the longitudinal steel (in the 7-foot (2.13-m) direction) underwent higher amounts of tension than the transverse steel (in the 6-foot (1.83-m) direction). This implies that the slab experienced higher stresses in the longer direction than in the shorter direction. This was also verified by the flexural cracks observed during testing which were perpendicular to the long direction.

6.1.1 Slab capacity — analytical vs. experimental. Before any experimentation, four different analytical procedures were used to estimate the capacities of the test specimens. For flexural capacity, a yield-line theory, typically utilized in the design of one-way and two-way slabs, was used. For punching shear capacity, three different methods were used: an ACI equation, an AASHTO equation, and a general punching shear model.

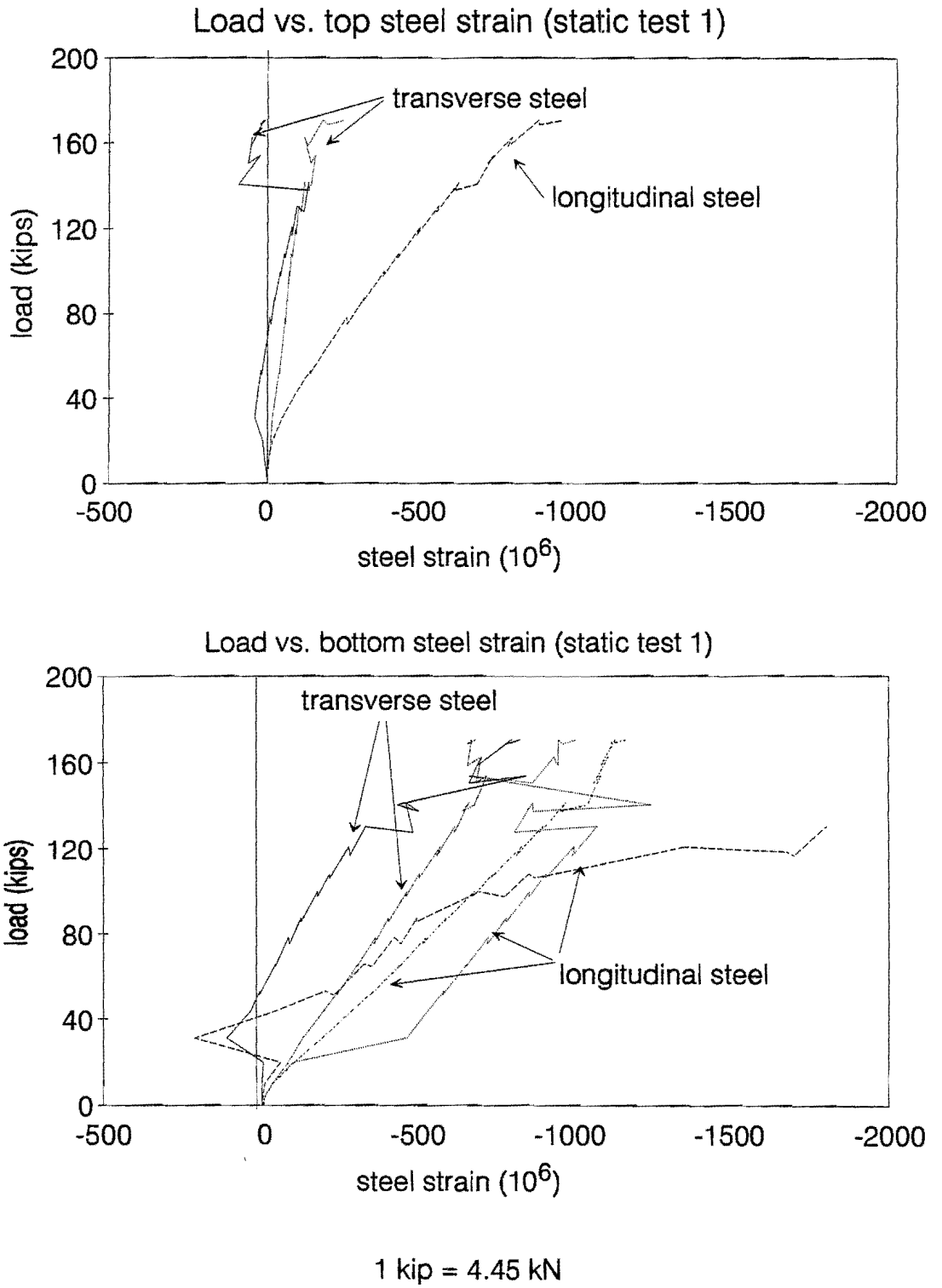

Figure 6.4 Load vs. steel strain for both top and bottom layers of reinforcing steel during static test of slab

The governing ACI equation (1989) is as follows [14]:

$$V_c = 4\sqrt{f_c}\, b_0\, d$$

The governing AASHTO (1983) equation is as follows [13]:

$$V_c = 2\,(\,0.8+\frac{2}{\beta_c}\,)\,(\,b_1+b_2+2d\,)\,d\,\sqrt{f_c} \quad < 1.8\sqrt{f_c}d\,(\,b_1+b_2+2d\,)$$

Where,

V_c = *punching shear load in lbs.*
f_c = *concrete compressive strength in psi*
b_0 = *perimeter of loading footprint*
d = *effective depth of section*
b_1, b_2 = *short and long side of loading footprint*
β_c = *ratio of* b_2 / b_1

The third punching shear equation is derived from a general punching shear model involving a truncated cone failure geometry, as described in Chapter 3. The equation for the general model is as follows [4]:

$$V_c = \frac{2d}{\tan\theta}\,(b_1+b_2+\frac{2d}{\tan\theta})\,f_t$$

Where,

θ = *angle of assumed failure plane (about 38 degrees)*
f_t = *tensile strength of concrete along assumed shear plane, or* $4\sqrt{f_c}$

The four estimated capacities, as well as the actual ultimate load from a static test, are shown in Figure 6.5. As shown, the AASHTO equation is very conservative, predicting only about 35 percent of the slab's true shear capacity. The ACI equation was closer to the actual capacity, but still quite conservative.

The general punching shear model predicted the actual capacity very accurately, and was conservative by less than 2 percent.

Also, it is worthy of note that punching shear controls over flexure in the slab. The flexural capacity from a yield-line analysis exceeds the slab's actual capacity by more than 20 percent.

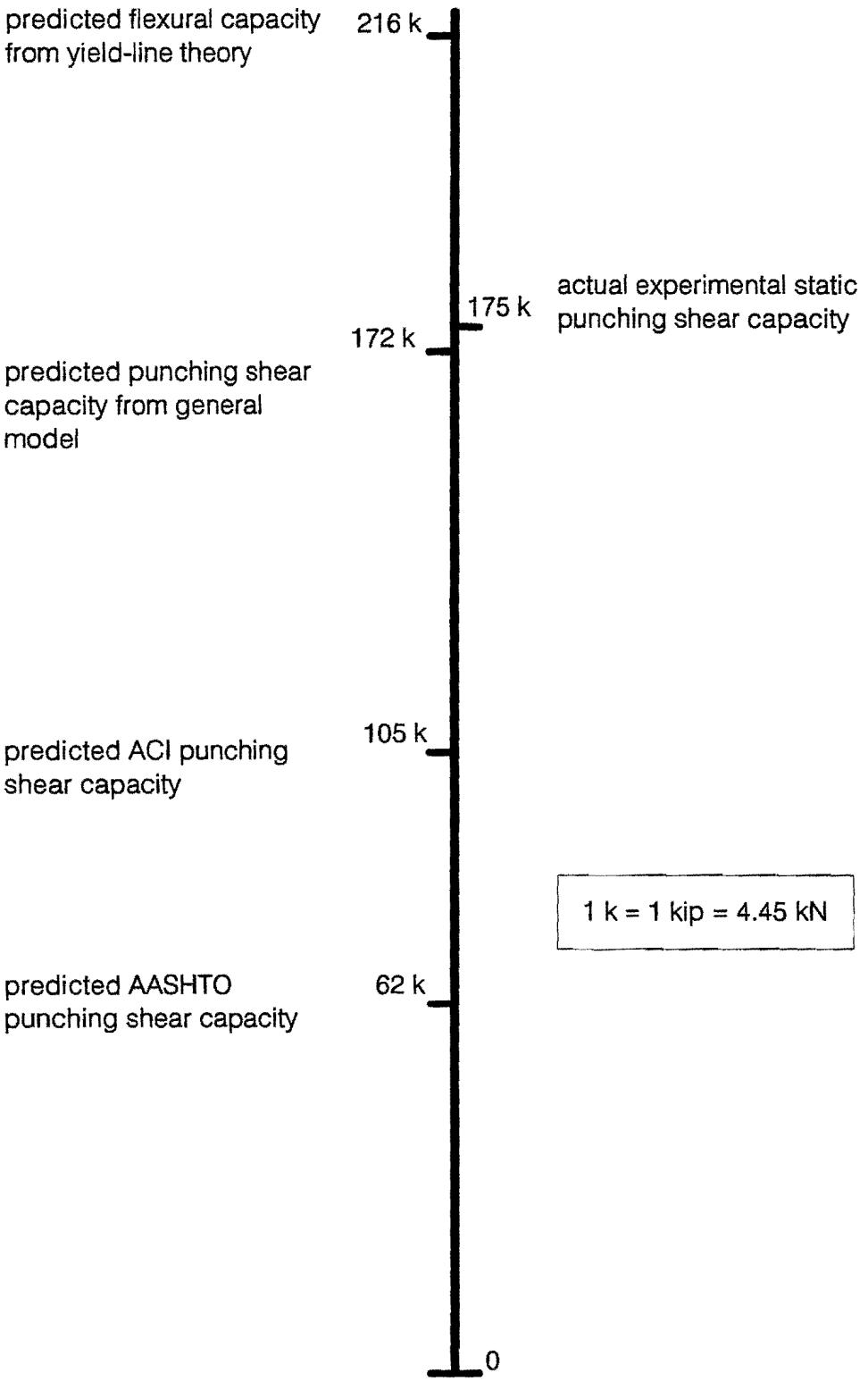

Figure 6.5 Comparison between predicted and observed slab capacity

6.2 Pulsating fatigue test results

As of this writing, a pulsating fatigue test had yet to be fully completed. Results and analyses will appear in future reports.

6.3 Rolling fatigue test results

As of this writing, a rolling fatigue test had yet to be fully completed. Results and analyses will appear in future reports.

CHAPTER 7
SUMMARY, CONCLUSIONS, AND RECOMMENDATIONS

7.1 Summary

The punching shear behavior of concrete bridge decks under static, pulsating fatigue, and rolling fatigue loads was studied using both analytical and experimental models. The study of the analytical models also played a large role in the design of the experimental specimens, test setup, and test procedure.

7.1.1 Analytical models. Two primary models were analyzed using the finite element method. The first model was a finite element mesh representing a full-size, realistic highway bridge. The prototype was a 50-foot-span (15.24-m), three-girder bridge with a 7.5-inch (191-mm) concrete deck. Solid elements, or 8-node brick elements, were used to model the concrete deck, while frame elements, or 2-node beam-column elements, were used to model the girders. This full-size bridge model was loaded in a typical AASHTO design truck loading pattern.

The second model represented the actual slab specimen to be tested in the laboratory. The full-scale specimen measured 6 feet (1.83 m) wide, 7 feet (2.13 m) long, and 7.5 inches (191 mm) thick, and was modeled using 8-node solid elements. Loading of the specimen model emulated the loading used in the experiment, which, in turn, was representative of an actual truck tire footprint.

When both models — the full-size bridge model and the experimental specimen model — were analyzed, it was observed that similar arching action behavior occurred in each, despite different geometries and load configurations. Also, it was possible to find out from the specimen model exactly how far a rolling load would have to move in order to obtain satisfactory fatigue behavior in the slab.

7.1.2 Experimental testing procedure. The steel testing frame for this project was designed for three different types of test: static loading, pulsating fatigue, and rolling fatigue. The static tests consisted of monotonically loading a full-scale slab until a punching shear failure occurred. The pulsating tests were very similar, but the load varied in magnitude, cycling until a punching shear failure occurred in the slab. The setup for the rolling tests was slightly different, allowing a constant load to be moved longitudinally across the slab, cycling until failure. Both types of fatigue tests were controlled through closed-loop servo-controllers and hydraulic loading systems.

As this report was being finalized, one complete static test had been completed. More static load tests, as well as several fatigue tests, are scheduled to be performed and will be discussed and analyzed in future reports.

7.2 Conclusions

The discussion above involved the development of an experimental program used to research the effects of fatigue on the punching shear capacity of a concrete bridge deck. From this developmental work, the following conclusions can be reached:

1) An experimental program and schedule was developed that, in time, will show fatigue effects on the punching shear resistance of concrete bridge decks.

2) A testing apparatus was designed to test concrete slabs in fatigue, both pulsating and rolling.

3) Using finite element analytical models of both full-size highway bridges and experimental specimens, the aforementioned setup and specimens were designed and constructed.

4) An initial static-load test of a full-scale concrete slab was conducted, and the general punching shear model used to estimate the slab's capacity was verified. Also, the controlling method of failure was indeed punching shear, as opposed to a flexural failure.

7.3 Recommendations

This report represents the work completed in the first 18 months of a three-year study. It is primarily meant to be a preliminary report discussing the analytical research, the planning of a testing scheme, the design and construction of a testing setup, and some initial results to verify analyses.

As of this writing, pulsating fatigue tests have begun, with rolling fatigue tests to follow. From these tests, S-N curves, as described above, will be produced, and the fatigue performance of the concrete slabs (as well as of the testing frame) will be verified.

At the end of this research project, a detailed report will be submitted describing all experimental results. These results will further verify (or discount) the results and analyses presented here. From the final results, recommendations will be made to the Texas Department of Transportation specifying the required thickness of bridge decks as a function of traffic characteristics.

REFERENCES

1. Ontario Highway Bridge Design Code and Commentary, Second Edition, Ontario Ministry of Transportation and Communication, Ontario, Canada, 1983.

2. Fang, I.-K., Worley, J., Klingner, R. E. and Burns, N. H., "Behavior of Ontario-Type Bridge Decks on Steel Girders," Research Report CTR 350-1, Center for Transportation Research, The University of Texas at Austin, January 1986.

3. Elling, C. W., Klingner, R. E. and Burns, N. H., "Distribution of Girder Loads in a Composite Highway Bridge," Research Report CTR 350-2, Center for Transportation Research, The University of Texas at Austin, January 1986.

4. Tsui, C. K.-T., Burns, N. H. and Klingner, R. E., "Behavior of Ontario-Type Bridge Decks on Steel Girders: Negative Moment Region and Load Capacity," Research Report CTR 350-3, Center for Transportation Research, The University of Texas at Austin, January 1986.

5. Kim, K. H., Klingner, R. E., Burns, N. H. and Dominguez, J., "Behavior of Skew Bridges with Ontario-Type Decks," Research Report CTR 350-4F, Center for Transportation Research, The University of Texas at Austin, January 1988.

6. Fang, I.-K., Worley, J., Klingner, R. E. and Burns, N. H., "Behavior of Isotropic Concrete Bridge Decks on Steel Girders," Structures Journal, ASCE, Vol. 116, No. 3, March 1990, pp. 659-679.

7. Fang, I.-K., Tsui, C. K.-T., Burns, N. H. and Klingner, R. E., "Fatigue Behavior of Cast-in-Place and Precast Panel Bridge Decks with Isotropic Reinforcement," PCI Journal, Vol. 35, No. 3, May-June 1990, pp. 28-39.

8. Klingner, R. E., Fang, I.-K., Tsui, C. K.-T. and Burns, N. H., "Load Capacity of Isotropically Reinforced, Cast-in-Place and Precast Panel Bridge Decks," PCI Journal, Vol. 35, No. 4, July-August 1990, pp. 104-114.

9. Perdikaris, P. C. and Beim, S., "RC Bridge Decks under Pulsating and Moving Load," ASCE, Journal of Structural Engineering, Vol. 114, No. 3, March 1988, pp. 591-607.

10. Perdikaris, P.C. Beim, S., and Bousias, S.N., "Slab Continuity Effect on Ultimate and Fatigue Strength of Reinforced Concrete Bridge Deck Models," ACI Structural Journal, Vol. 86, No. 4, July-August 1989, pp. 483-491.

11. Wilson, E., and Habibullah, A., "SAP90™ -- A Series of Computer Programs for the Static and Dynamic Finite Element Analysis of Structures," Computers and Structures, Inc., Berkeley, California, 1990.

12. Johnston, P.R., and Weaver, W., Finite Elements for Structural Analysis, 1984.

13. Standard Specifications for Highway Bridges, 13th edition, American Association of State Highway and Transportation Officials, 1983.

14. Building Code Requirements for Reinforced Concrete and Commentary, American Concrete Institute, ACI 318-89 and ACI 318R-89.